Dental Materials Journal 2008; 27(4): 485−498

Original Paper

Non-linear Viscoelastic Finite Element Analysis of the Effect of the Length of Glass Fiber Posts on the Biomechanical Behaviour of Directly Restored Incisors and Surrounding Alveolar Bone

Marco FERRARI[1], Roberto SORRENTINO[1,2], Fernando ZARONE[2], Davide APICELLA[3], Raffaella AVERSA[4] and Antonio APICELLA[5]

[1]*Department of Dental Materials and Restorative Dentistry, University of Siena, Italy*
[2]*Department of Fixed Prosthodontics, University of Naples "Federico II", Italy*
[3]*Department of Operative Dentistry, Second University of Naples (SUN), Italy*
[4]*Department of Materials Engineering and Productions, University of Naples "Federico II", Italy*
[5]*DISPAMA, Materials Laboratory, Second University of Naples, Italy*
Corresponding author, Marco Ferrari; E-mail: md3972@mclink.it

The study aimed at estimating the effect of insertion length of posts with composite restorations on stress and strain distributions in central incisors and surrounding bone.

The typical, average geometries were generated in a FEA environment. Dentin was considered as an elastic orthotropic material, and periodontal ligament was coupled with nonlinear viscoelastic mechanical properties. The model was then validated with experimental data on displacement of incisors from published literature. Three post lengths were investigated in this study: root insertion of 5, 7, and 9 mm. For control, a sound incisor model was generated. Then, a tearing load of 50 N was applied to both sound tooth and simulation models.

Post restorations did not seem to affect the strain distribution in bone when compared to the control. All simulated post restorations affected incisor biomechanics and reduced the root's deforming capability, while the composite crowns underwent a higher degree of deformation than the sound crown. No differences could be noticed in incisor stress and strain. As for the influence of post length, it was not shown to affect the biomechanics of restored teeth.

Key words: Periodontal ligament viscoelasticity, Post length, Finite element analysis

Received Nov 2, 2007: Accepted Jan 16, 2008

INTRODUCTION

Fractures frequently occur in endodontically treated teeth[1,2]. Fiber posts are effective in withstanding compressive loads, as in the case of posterior tooth restorations[3]. However, their flexural behavior should be carefully considered under non-axial loads, as in the case of incisors[4]. In post and core restorations, stress distribution within the structure is multiaxial, not uniform, and depending on the magnitude and direction of the applied external load[5]. Type of external loading, geometry of structure, and residual stresses are some of the causes of multiaxial stress distributions[6]. Furthermore, the mechanical behavior of post and core-treated teeth is influenced by the characteristics of the interfaces and the rigidity of the materials[7]. The use of glass fiber posts has resulted in stress distributions similar to those in sound teeth due to the increased deformability of the root[8-11]. Nonetheless, some of the fractures affecting post restorations could be related to a concentration of forces[12]. On this note, fatigue loading must be considered as an additional cause of root fracture.

To date, there is still no agreement in the literature about which material or technique can optimally restore endodontically treated teeth[13]. Post length remains one of the most controversial topics. Obviously, the deeper the post length, the more dentin will be removed, thereby potentially weakening the root[14]. Moreover, the deeper the post insertion, the more difficult it will be to achieve a reliable adhesion. This occurs due to twofold reasons: anatomical constraints (*i.e.*, reduction of dentinal tubules in mm^2 in the apical direction) and technical difficulties (*i.e.*, limited detersion and accumulation of canal wall debris in the apical third)[15]. Conversely, according to some studies, a decrease in post length would provide less retention to the post itself and an increase in dentinal stress[16,17]. On post lengths, it is commonly recommended to be equal to ¾ of root canal length or at least equal to the length of the crown[18], leaving at least 4 mm of gutta-percha at the level of the apex to provide a reliable apical seal[19].

To validate the clinical effectiveness and predict the long-term success of restorative systems, it is of paramount importance to have a proper understanding of the physical variables affecting the mechanical behavior of biomaterials[11]. The Finite Element

Analysis (FEA) tool allows researchers to achieve detailed evaluations of the mechanical behaviors of biologic and/or restorative systems, even in non-homogeneous bodies[11,20-22]. If correctly validated, the FEA could be useful in optimizing restorative design criteria and material choice and in predicting potential fracture under given circumstances[11].

Most of the FEA studies on the strain and stress distribution in post and crown-restored teeth are based on two-dimensional (2D) models[23-25], with only a few on three-dimensional (3D) ones[8,11,17,26]. Although reliable when considering axial symmetric systems, 2D meshing procedures do not allow correct assessment of the spatial distribution of stresses and strains affecting a restorative system. To overcome such a problem, 3D FEA was introduced to obtain more realistic models[8,11].

The present study compared the stress and strain distribution patterns of a sound maxillary central incisor with those of endodontically treated teeth restored with different post lengths. The aim of the present study was to investigate the influence of post lengths on the biomechanical behavior of restored teeth, periodontal ligament (PDL), and alveolar bone. The following null hypothesis was tested: there is no association between the length of fiber posts and the stress and strain concentration areas within the restored teeth, PDL, and alveolar bone. On clinical significance, the results of the present study would allow clinicians to make an informed choice when preparing the dowel space to a certain length.

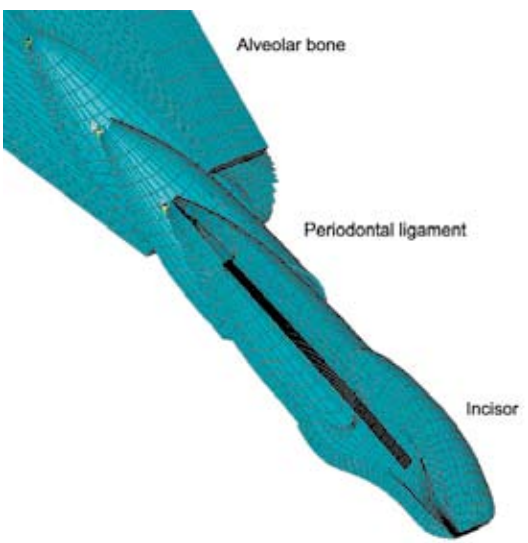

Fig. 1 FE models of the maxillary central incisor, PDL, and alveolar bone.

MATERIALS AND METHODS

Generation of finite element models

The solid model consisted of a maxillary central incisor, PDL, and the anterior part of the maxillary cortical and cancellous bone. The incisor's solid model was generated using literature data[21] for dentin and enamel in terms of internal volumes and morphologies, while the external shape of the maxillary central incisor was obtained by laser-based 3D digitizing (Cyberware Inc., Monterey, CA, USA) of a plaster cast (Thanaka manufacturer, Tokyo, Japan). Scanned profiles were assembled into a 3D wire frame structure using a 3D CAD tool (AutoCAD 12, Autodesk Inc., San Rafael, CA, USA) and exported into a 3D parametric solid modeler (Pro-Engineering 16.0, Parametric Technologies, Needham, MA, USA). Tooth volumes were generated by fitting the horizontal and vertical profiles.

The average anatomical dimensions of the bone in adults were generated according to literature data[27]. The maxillary bone was modeled as a cancellous core surrounded by 2.0-mm-thick cortical bone. The bucco-lingual and anterior-posterior lengths of the bone models were 7.3 mm and 13 mm respectively at the root apex level. An average thickness of 0.7 mm was considered for the alveolar cortex[28]. An average thickness of 0.2 mm was considered for the PDL[29]. Besides, the different geometries of post and cement layer were also modeled at this step.

The FE model was obtained by importing the

Table 1 Mechanical properties of tissues and materials

Material/component	Young's modulus (GPa)	Poisson's ratio
Dental pulp	0.1e-04	0.3
Enamel	84.1	0.33
Cementum	18.7	0.3
Cancellous bone	0.91	0.22
Cortical bone	10.7	0.3
Gutta-percha	0.96 e-03	0.3
Composite (Gradia forte)	13.7	0.3
Cement (Unifil Core)	13	0.22
Adhesive	1	0.3

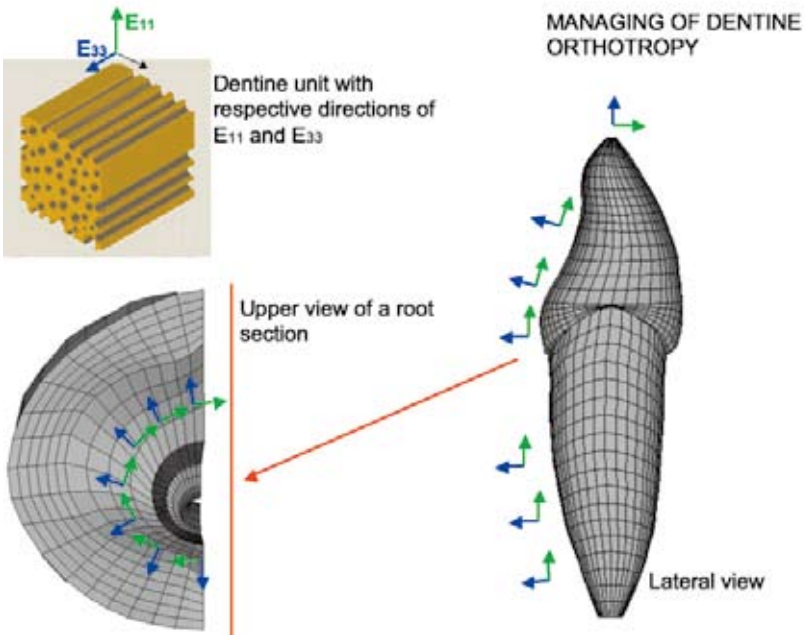

Fig. 2 Managing dentin orthotropy: orientation of E_{11} and E_{33} with respect to a dentin micro-unit. Orientation of local coordinate systems in the sagittal and transversal planes. Elements coordinate systems were oriented with respect to the shown coordinate systems.

Table 2 Orthotropic properties of dentin. Young's moduli (E expressed in GPa), Poisson's ratios (ν), and shear moduli (G expressed in GPa)

E_{11} (GPa)	25
E_{33} (GPa)	23.2
ν_{21}	0.45
ν_{31}	0.29
G_{12} (GPa)	8.6
G_{23} (GPa)	9.4

solid models into ANSYS rel. 9.0 FEM software (Ansys Inc., Canonsburg, PA, USA) using IGES format. The volumes were redefined in the new environment and meshed with 8-node brick with 3 degrees of freedom per node, resulting in a 3D FE model made up of 31,240 elements and 35,841 nodes (Fig. 1). The model was constrained at the top surface of the maxillary bone, coupled with symmetry constraints on the medial side. Accuracy of the model was checked by convergence tests.

Materials properties

1) Natural tissues

Enamel, cementum, gutta-percha, cancellous and cortical bone were considered as isotropic elastic materials. Their mechanical properties are summarized in Table 1[30-34]. As reviewed by Kinney *et al.*[35], an orthotropic symmetry better describes the effects of tubular orientation and disposition of collagen fibrils orthogonal to the tubules on dentin microstructure.

An orthotropic structure has nine independent elastic constants. By convention, the nine elastic constants in orthotropic constitutive equations comprised three Young's moduli (E_{11}, E_{22}, E_{33}), three Poisson's ratios (ν_{23}, ν_{31}, ν_{12}), and three shear moduli (G_{23}, G_{31}, G_{12}). The Young's moduli E_{11}, E_{22} measured in orientations orthogonal to the tubular axis (the principal structural directions) were identical, but the modulus E_{33} parallel to the tubular axis was determined to be lower[35]. Table 2 lists the values of the elastic constants used in this study.

Figure 2 is a schematic local reproduction of maximum (E_{11}, E_{22}) and minimum stiffness (E_{33}) orientation assumed in our study with respect to dentin microstructure. Moreover, the effect of tubular orientation on the mechanical behavior of the incisor model was managed as follows. A series of local coordinate systems were generated along the incisor model. They were oriented in the FE environment according to the tubules' direction extrapolated by histological sections of an incisor on the sagittal and horizontal planes. Dentin elements' coordinate systems in a given area were oriented with respect to the nearest local coordinate system. A schematic view of the local coordinate systems' disposition is presented in Fig. 2 on the sagittal and horizontal planes respectively.

2) Time dependency of PDL

Available clinical and experimental evidences indicate that the response of PDL is both elastic and

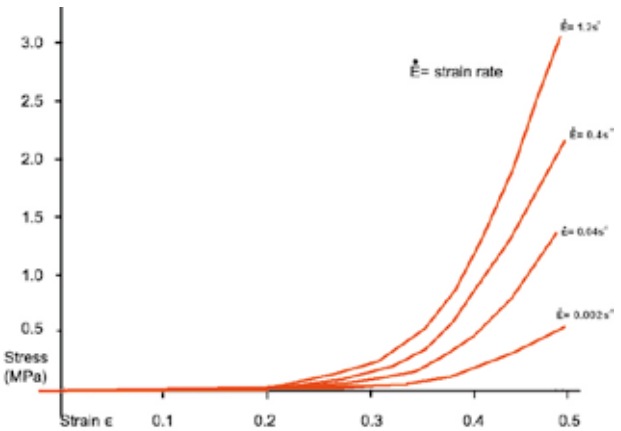

Fig. 3 PDL stress-strain curves performed at different straining rates.

Table 3 Orthotropic properties of glass fiber posts. Young's moduli (E expressed in GPa), Poisson's ratios (ν), and shear moduli (G expressed in GPa).

E_x (GPa)	37
E_y (GPa)	9.5
E_z (GPa)	9.5
ν_{xy}	0.27
ν_{xz}	0.34
ν_{yz}	0.27
G_{xy} (GPa)	3.1
G_{xz} (GPa)	3.5
G_{yz} (GPa)	3.1

viscous[36,37]. Time dependency characterizes the viscosity in contrast with elasticity in which all deformations are instantaneous. It is commonly accepted that the PDL's elastic component is nonlinear. Recently, some authors demonstrated that the viscous component is also governed by a nonlinear behavior[38]. The effect of the elastic component's nonlinearity on the stress-strain curve is a stiffening at higher deformation levels. Conversely, the effect of the viscous component's nonlinearity on PDL's stress-strain curves is a stiffening at higher straining rates and which could not be described by a constant strain rate hardening parameter.

The method used to account for the strain rate dependency of stress required the definition of five viscoelastic models based on five different stress-strain curves performed at different straining rates. Literature data about bovine PDL's stress-strain curves performed at different straining rates[38] were used to set up the viscoelastic models. These models consisted of "bulk modulus *versus* time" curves. Once the strain rate of a given stress-strain curve is known, it is possible to evaluate for a discrete number of its points a series of bulk moduli corresponding to the different time steps of the performed experiment.

In the present study, a "bulk modulus *versus* time" curve was evaluated for each stress-strain curve. Data were uploaded to the FEA software. A macro was set up in order to enable a time-dependent analysis that computed at each sub step time the strain rate of a given element. The strain value and the corresponding strain rate were interpolated between the "nearest" viscoelastic models to determine the corresponding stress value. Figure 3 shows the stress-strain curves at different straining rates as obtained from the literature. Although the bovine PDL is wider than human PDL, their compositions seem to be comparable[39]. In previous studies[40-42], the bovine model has been considered as a promising approach to define the main parameters responsible for the mechanical behavior of human PDL.

3) Restorative materials

A high-rigidity composite material (Gradia Forte, GC Corp., Tokyo, Japan) was considered for the restored crowns of MOD 2, 3, and 4. The composite material was considered isotropic and its mechanical properties are listed in Table 1. Posts were made of unidirectional glass fiber (Young's modulus: 70−75 GPa) embedded in a resin matrix (1.5−2 GPa) and oriented along the post's longitudinal axis. Elastic orthotropic properties are derived from the Halpin-Tsai equations for fiber-reinforced composite materials[43] for transverse (minimum stiffness: E_y, E_z) and axial directions (maximum stiffness: E_x), as given in Table 3.

4) Test models

This study comprised four test models designated as MOD 1, MOD 2, MOD 3, and MOD 4. A quick overview of these test models is given below.

- Model 1 (MOD 1): FE model of a sound maxillary central incisor with PDL and surrounding alveolar bone.
- Model 2 (MOD 2): FE model of a maxillary central incisor with PDL and surrounding alveolar bone restored with a glass fiber post with 9 mm endo-canalar length and a composite crown.
- Model 3 (MOD 3): FE model of a maxillary central incisor with PDL and surrounding alveolar bone restored with a glass fiber post with 7 mm endo-canalar length and a composite crown.
- Model 4 (MOD 4): FE model of a maxillary central incisor with PDL and surrounding alveolar bone restored with a glass fiber post with 5 mm endo-canalar length and a composite crown.

Relative distances between the post and the anatomical structure are summarized in Fig. 4.

5) Adhesive layers

Adhesive layers were modeled in the FE environment using spring elements[44] to connect the nodes from the post surface to the cement layer (interface A), from the dentin side of the cement layer (interface B), from the crown composite surface to the dentin surface (interface C), and from the composite crown to the post structure (interface D) (Fig. 5). Normal and shear stiffness of the adhesive layers were simulated by connecting each pair of nodes with three different springs: one in the direction normal to the simulated interface and the other two parallel to the interface. The spring constant *Ki* for the element normal to the interface layer was determined using the following formula:

$$Ki=AiE/l$$

where *Ai* is the nodal average area evaluated as the average value of the concurring element areas to each node, *E* is the Young's modulus of the adhesive material, and *l* is the thickness of the interface (50 μm).

A nodal average value for the area was assumed in order to obtain a homogeneously distributed rigidity inside the adhesive, overcoming the effect of non-homogeneity or edge presence of the mesh. For the springs placed in the interface plane, the rigidity was defined as $Ki=AiG/l$, where *G* is the shear modulus of the adhesive material. For each pair of nodes, the two springs parallel to the interface had the same rigidity. The material properties of the adhesive were: Young's modulus at 1 GPa and Poisson's ratio at 0.3[44].

6) Applied loads and model validation

To reproduce a dynamic loading effect, a transient analysis with time integration was used. Each load reached the maximum assigned value through defined load steps at different times.

Short-term intrusive load: Intrusive displacement was calculated by referring to a chewing activity of 70 cycles per minute (Fig. 6)[29,45]. Parfitt's experimental test was reproduced in the FE environment by applying an intrusive load of 3 N. The intrusive load was gradually increased up to 3 N (0.5 N for each load step of 0.14 seconds) within an overall time interval of 0.85 seconds. The resulting displacement in the direction of the load was measured and compared with experimental data (Fig. 7).

Horizontal load: The horizontal load was gradually increased up to 15 N (1 N for each load step of 5 seconds) within an overall interval of 75 seconds (Fig. 6). Displacement in the direction of the load was measured and compared with experimental data[46] and computed data from published

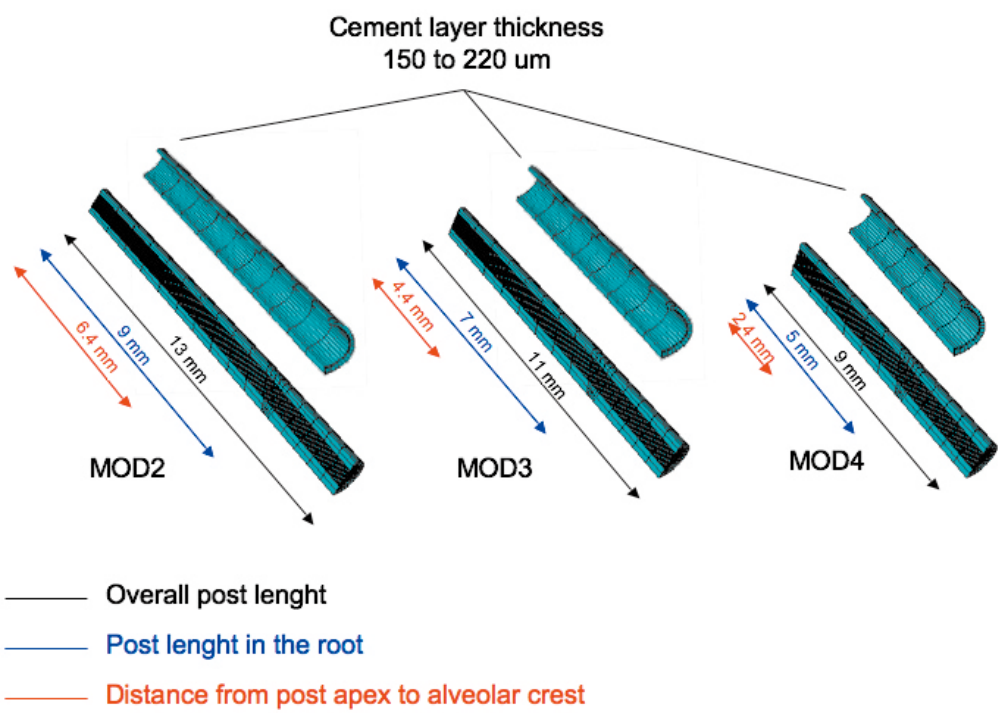

Fig. 4 Tested post dimensions, post insertion in the root, and distance between post apex and alveolar crest.

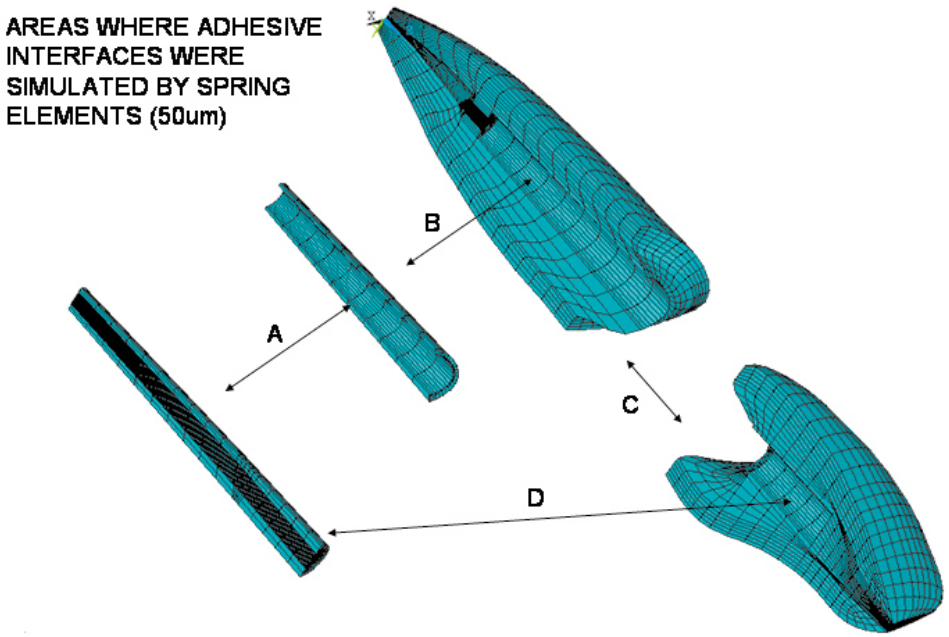

Fig. 5 Areas where interface were modeled using spring elements.

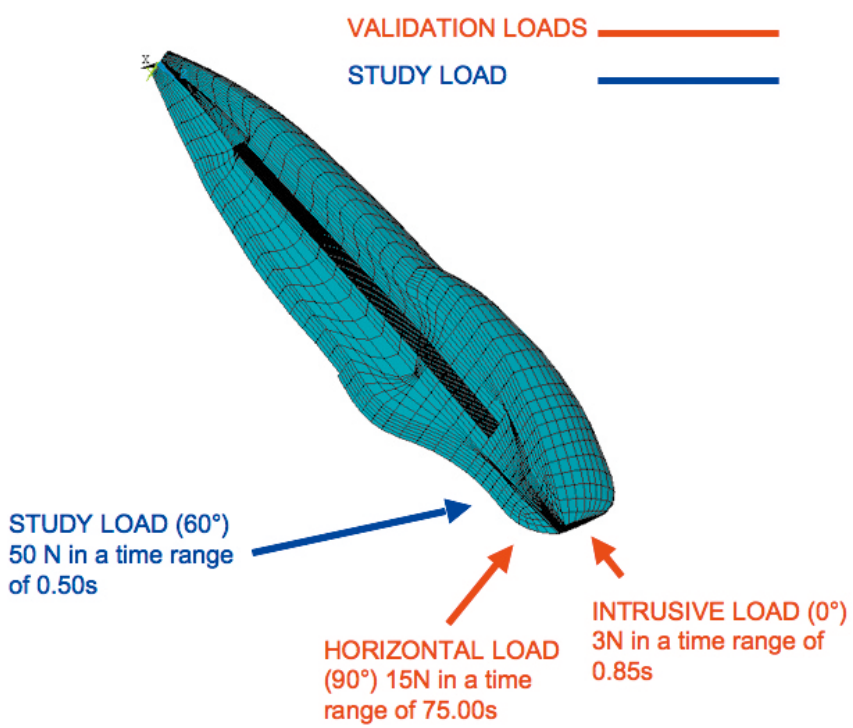

Fig. 6 Applied loads and relative directions. Loads used for model validation are reported in red; load applied to simulate the tearing function is reported in blue.

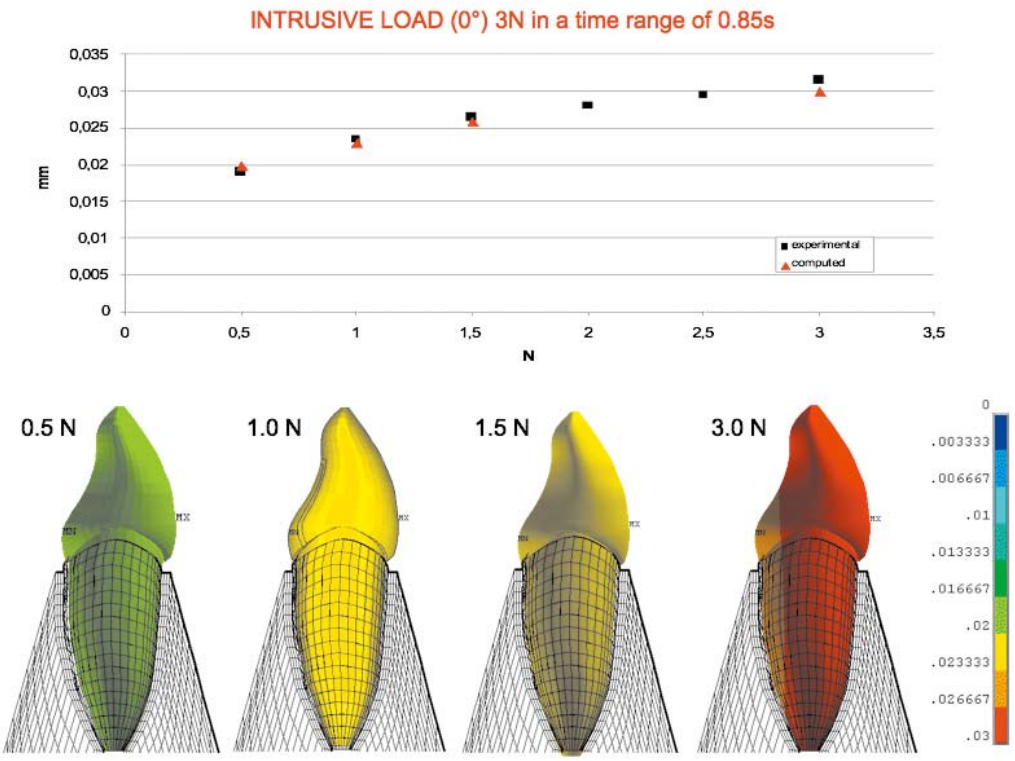

Fig. 7 Validation diagram for intrusive load. Recorded displacements are compared to experimental displacements recorded in the same loading conditions from published literature.

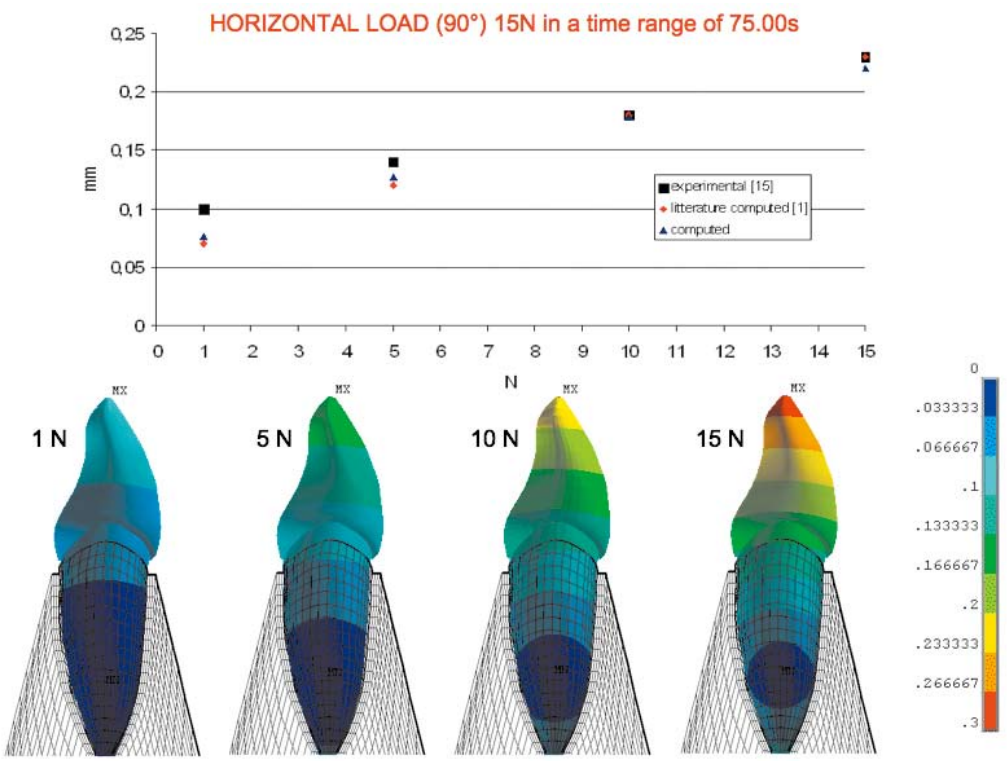

Fig. 8 Validation diagram for horizontal load. Recorded displacements are compared to experimental displacements recorded in the same loading conditions from published literature.

literature[27]. Figure 8 shows the computed displacements at 1, 5, 10, and 15 N.

Study load: For the final analysis, a load was applied at 60° angle to the tooth's longitudinal axis. Load application was on the palatal surface of the crown at 2 mm apically to the incisal margin. Applied load was increased up to 50 N within a time interval of 0.5 seconds to simulate a tearing function.

RESULTS

Figure 9 shows the von Mises strain values within the cancellous and cortical bone. A gradient triad display style was used to visualize the state of strain response within the incisor-alveolar system in a 3D manner. For all the models, the highest strain value for the spongy bone (0.003 ε) was recorded on the cervical margin of the alveolar ridge (yellow arrows in Fig. 9). The strain values progressively decreased in coronal-apical direction. A similar behavior was noted in all the models for the cortical bone, where the highest strain value (0.0015 ε) was recorded along the cervical margin of the alveolar ridge (red arrows in Fig. 9). For all the models, strain values along the thin cortical layer surrounding the PDL ranged from 0.0015 to 0.00185 ε.

Figure 10 shows the von Mises strain distributions along the PDL structure for all the test models. On the average, the PDL was strained to 0.1 ε. The highest strain value (0.5 ε) for PDL was noted in all the models to be near the cervical area and its apical region. Von Mises strain distributions within the sound and restored incisors are presented in Fig. 11.

For MOD 1, the strain level in the cervical region was higher when compared to MOD 2, 3, and 4. On the contrary, non-appreciable differences in strain level were noted in this region between MOD 2, 3, and 4. For all the models, the highest strain value (0.9 e−03 ε) was recorded in the cervical area of root dentin on both the palatal and buccal sides. Moreover, strain values within the root structure progressively increased from the central longitudinal axis (0.113e−03 ε) to the palatal and buccal sides of the outer surfaces (0.675e−03 ε).

At the crown structure, the highest strain value (0.225e−03 ε) for the sound incisor was recorded on the buccal and palatal regions of the crown. Conversely, strain values for restored models ranged from 0.788e−03 ε in the crown cervical region to 0.113e−03 ε in the incisal margin.

Figure 12 shows the $\sigma 1$ principal stress distributions in all the test models. The principal stresses were ordered such that $\sigma 1$ rendered the most positive value (tensile) and $\sigma 3$ rendered the most negative value (compressive). For all the models, the highest tensile stress of 30 MPa was recorded in the cervical region of the root dentin on the palatal side (as indicated by the red arrows). Moreover, tensile

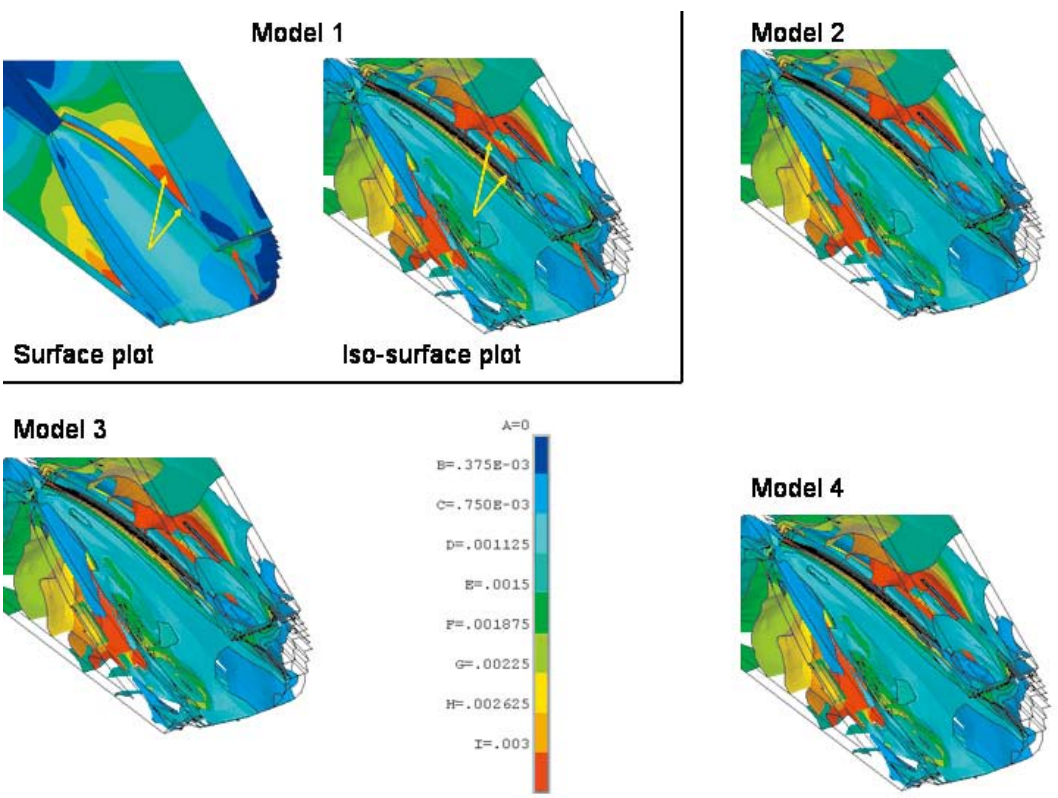

Fig. 9 Von Mises strain distributions in the alveolar bone for Models 1−4. Values are expressed in ε.

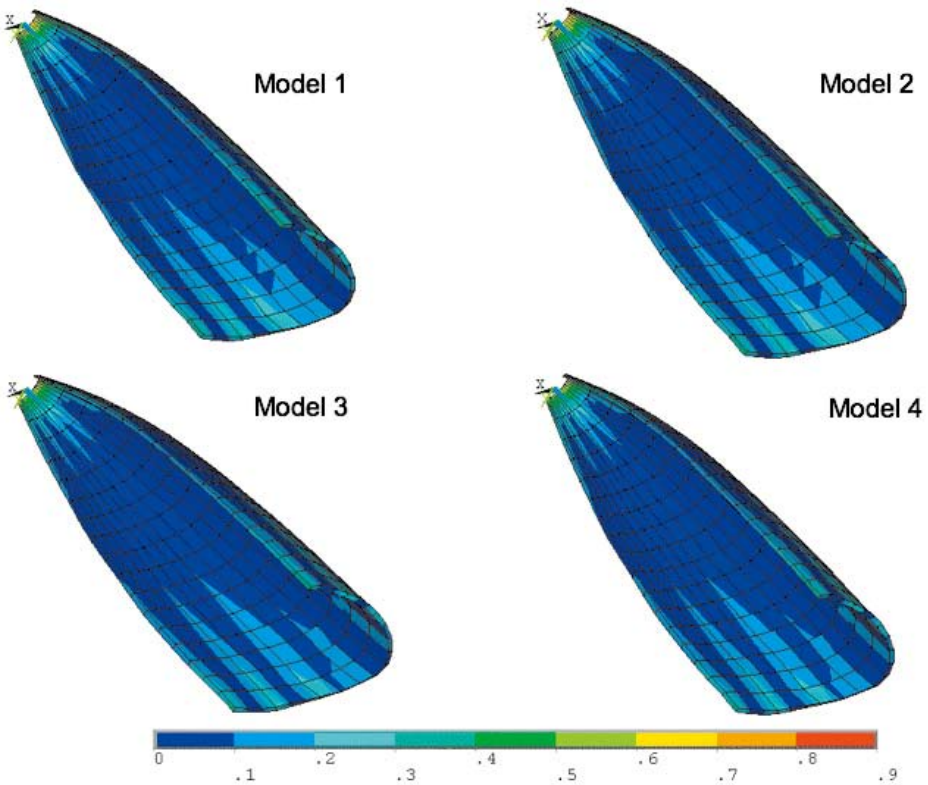

Fig. 10 Von Mises strain distributions in the PDL layer for Models 1−4. Values are expressed in ε.

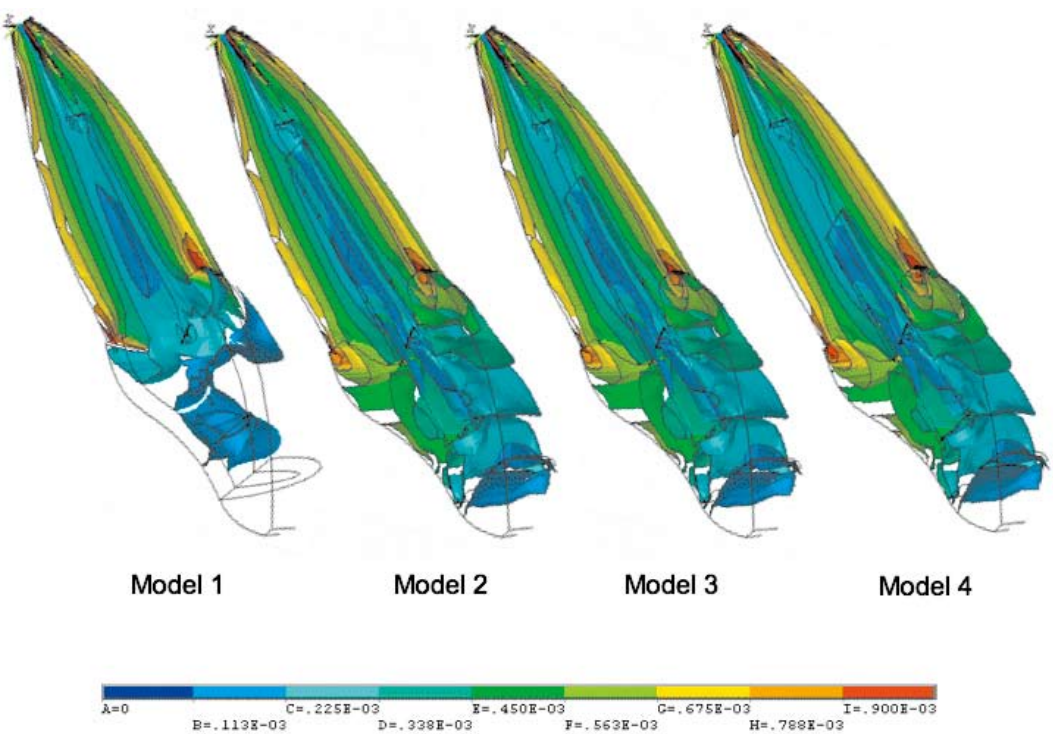

Fig. 11 Von Mises strain distributions in the incisor structure for Models 1−4. Values are expressed in ε.

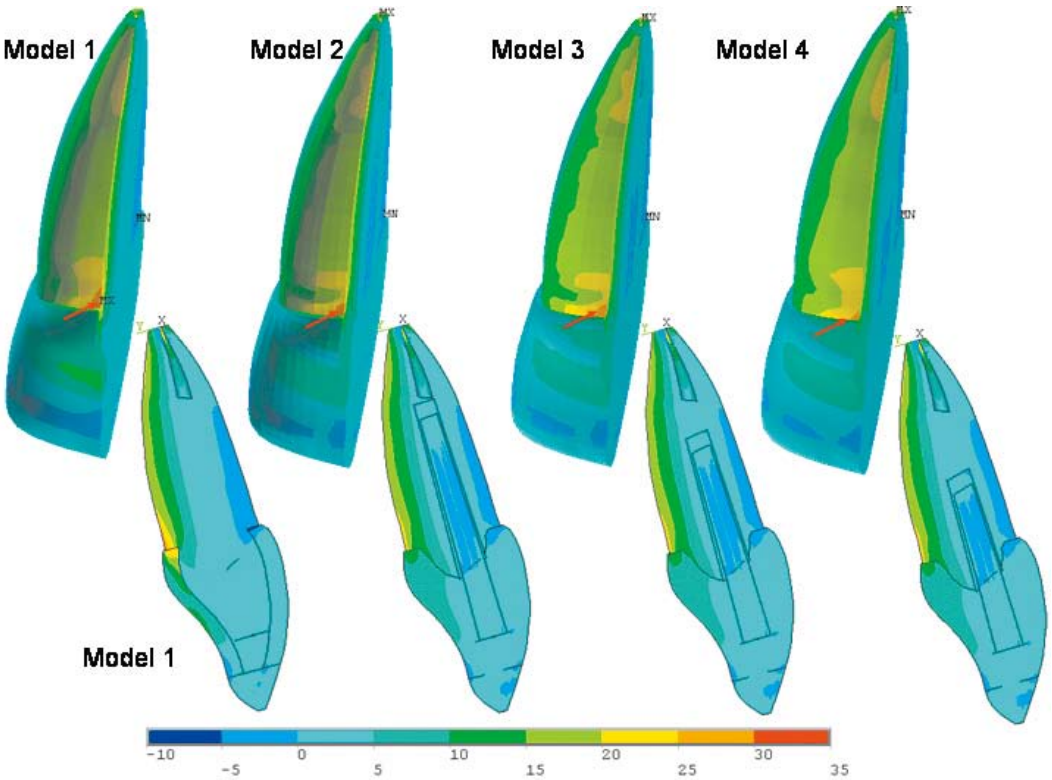

Fig. 12 σ1 principal stress (tensile stress) in the incisor structure for Models 1−4. Values are expressed in MPa.

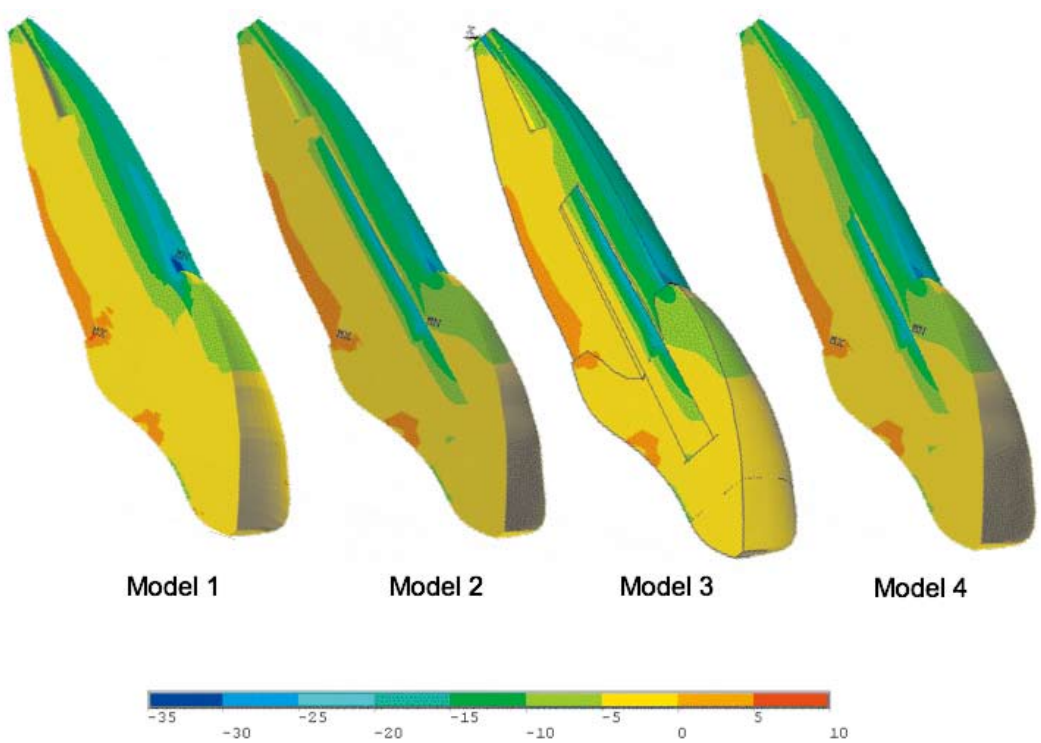

Fig. 13 σ3 principal stress (compressive stress) in the incisor structure for Models 1−4. Values are expressed in MPa.

stress values along the overall palatal surface of the root ranged from 15 to 20 MPa. At the crown structure, tensile stress in the sound model ranged from 5 to 15 MPa, while that in the restored models ranged from 5 to 10 MPa.

Figure 13 shows the $\sigma 3$ principal stress distributions in all the test models. The highest compressive stress values were noted for all the models on the buccal side of the root cervical area (−35 MPa for sound model; −30 MPa for restored models). For all the models, compressive stress values along the overall buccal surface of the root ranged from −15 to −25 MPa. At the crown structure, compressive stresses ranged from −10 to −25 MPa in the cervical region for the sound model. Conversely, for the restored models, compressive stresses ranged from −10 to −15 MPa.

DISCUSSION

The present study was designed to obtain a biofaithful model of the maxillary incisor system (incisor, PDL, alveolar bone) and to assess the effect of glass fiber post lengths on the overall system's biomechanics. The use of spring elements to simulate the interfaces was achieved exclusively to enable the overall system to behave like a "bonded system".

All the test models (sound incisor and restored incisors) showed comparable strain patterns in the alveolar system (compact and spongy bone) (Fig. 9). The overall system's strain pattern did not appear to be influenced by post length. Von Mises strain values along the PDL structure were comparable for all the test models (Fig. 10). The highest recorded strain value of the PDL (0.5 ε) entailed the physiological deformability of the PDL structure[40].

Dissipation of energy was achieved by the bending of the overall system in which four main phenomena occurred: the spongy bone was compressed on one side and stretched on the other, the bending of the cortical bone's knife edges, the bending of the tooth, and the deformation of the PDL layer.

The initial high deformability of the PDL (corresponding to the nonlinear slope of the PDL's stress-strain curve) allowed a high displacement of the incisor in the alveolar socket. Therefore, a large amount of energy produced by the tearing load was dissipated during the early stage of the loading history through PDL deformation. When a PDL strain level of 0.4 ε was overcome, the fibers were stretched and PDL rigidity reached its maximum value. At this stage, the PDL behaved like an elastic material (straight dominium of the stress-strain curve). At the same time, a larger amount of energy was transferred to the surrounding alveolar bone, such that the alveolar support consequentially participated in the incisor bending movement in the palatal-buccal direction. Such behavior was due to the alveolar morphology characterized by a knife edge-like morphology. The progressive alveolar bone thinning in the coronal-apical direction significantly increased the deformability of the alveolar bone's knife edge, resulting in a larger amount of strain in these areas.

Due to the transverse-applied loads, the displacements transferred to the post were orthogonal to its fibers. The post's rigidity in the direction orthogonal to fibers was significantly lower than that of the surrounding dentine (*i.e.*, 9.5 *versus* 23 GPa, Table 3). Deformation orthogonal to the post was not significantly influenced by the post's rigidity. In view of the results obtained, post length did not seem to affect stress values in the surrounding root dentin.

Further, such results suggested that the PDL could compensate for increased tooth rigidity (as in the case of a post restoration). This was achieved by enabling the incisor to move like a rigid body within the alveolar socket (no bending of the incisor) in the early stage of the loading history and limiting the bending phenomenon to occur in the final steps of the loading history. A great part of the energy was dissipated during PDL deformation, but a lower amount during incisor bending. In the latter condition, the post length played a secondary role whereby the main part of the phenomenon was produced by dentin compression and tension on both the palatal and buccal sides. Therefore, the highest strain level was noted in the cervical region of the root dentin on both the palatal and buccal sides in all the test models, which was due to incisor bending under the applied load (Fig. 11).

The strain level in the cervical region depended on several factors. On one hand, factors at play included the root portion inserted in the alveolar bone, root dentin's mechanical properties, PDL's thickness and mechanical properties, as well as the geometries of alveolar cortical and spongy bone and their mechanical properties. On the other hand, the strain level depended on the crown geometry (whereby the strain values were constant in all the test models) and the mechanical properties of the crown materials (which were constant for MOD 2, 3, and 4 but different for MOD 1). In light of these results, it could be hypothesized that observed differences in the strain level in the root dentin's cervical area between MOD 1 and MOD 2, 3, and 4 were due to differences in the mechanical properties of the crown materials more than the geometries of the different posts that characterized MOD 2, 3, and 4.

Such hypothesis was based on the evidence that there were no differences in the strain level between

MOD 2, 3, and 4 in the cervical region and in the other areas of the restored teeth. Conversely, the differences in strain level in the cervical area between MOD 1 and MOD 2, 3, and 4 could be explained by a discontinuity in terms of crown material's mechanical properties. The Young's and shear moduli of the enamel layer were significantly higher when compared to those of the composite restorative materials. Similarly, the values of both the orthogonal Young's and shear moduli of the crown dentin were almost twice of those of the composite restorative materials. The higher stiffness of the sound crown resulted in a lower amount of strain in the crown body, whereas the lower stiffness of the restored crown resulted in a higher amount of strain in the restored crowns body. Stated differently, the sound crown deformed like a rigid body and transferred the deformation to the root dentin in the cervical area; on the other hand, the composite-restored crowns of MOD 2, 3, and 4 bent under the applied load and transferred the lower strain to the root dentin in the cervical area.

On the influence of cement layer thickness on stress distributions, it remains controversial and debatable. In the present study, a simple root canal anatomy was simulated whereby cement layer thickness was assumed to be uniform and consistent along the entire fiber post. Conversely, the shapes of root canals vary in clinical conditions, which means that cement layer thickness will be inevitably higher at some areas than at other areas. At present, it remains to be confirmed if stress distribution along a fiber post is indeed influenced by this irregularity.

With regard to the root structure, tensile stress ($\sigma 1$) in all the test models prevailed on the palatal side (Fig. 12), whereas compressive stress ($\sigma 3$) prevailed on the buccal side (Fig. 13). In both cases, stress concentration areas in Figs. 12 and 13 corresponded to the strain concentration areas in Fig. 11. This behavior was thus consistent with the linear relationship between stress and strain assumed for the dentin structure[35]. Assuming general linear elasticity behavior, the relationship between stress and strain tensors is given as follows:

$$\sigma = [E/(1-\nu^2)C](\varepsilon - \varepsilon_0) + \sigma_0 \qquad (1)$$

where σ is the stress tensor, ε is the strain tensor, E is the Young's modulus, ν is the Poisson's ratio, and C is the stiffness matrix. According to Equation (1), a low stress value for a given strain will result in decreased stiffness for the material (*i.e.*, E=84 GPa and E=13 GPa for sound enamel and composite crown respectively). Accordingly to Equation (1), the dissimilar stress reactions between the sound and restored models could then be attributed to the concomitant mismatch in mechanical properties.

Principal stress σ_1 values recorded in the post structure and cement layer were comparable with those recorded in the surrounding dentin. On one hand, the absence of relevant tensile stress in the areas where multiple interfaces existed suggested that low tension was transferred to the interfaces. On the other hand, we maintained that the "interface problem" should be examined with a sub-modeling approach at these areas. In this sense, the current preliminary analysis on the overall system's biomechanics would be useful and could be leveraged for the sub-modeling study.

For most materials, the compressive strength is greater than the tensile strength. Unidirectional fiber-reinforced composites are among the very few materials that exhibit a greater tensile strength than compressive strength. This behavior stems from a compressive failure mechanism in fiber composites in the form of microbuckling. Microbuckling can occur on one side due to a local instability of fibers, and on the other side by the yielding of shear deformation in the composite in connection with initially misaligned fibers[47].

The failure of a fiber post during a flexural deformation is due to the microbuckling of fibers on the side where the load is applied and where severe fiber compression occurs. Nevertheless, stress values recorded in the present model were significantly below the flexural strength of fiber posts reported in other studies (from 565 to 898 MPa)[48].

During physiological occlusal and masticatory functions, both natural and restored teeth are subjected to cyclic loading. Therefore, failure due to fatigue stress is a very important and serious concern from a clinical standpoint[49-51].

It is commonly accepted that unidirectional fiber-reinforced composites have very promising static ultimate properties. Conversely, their fatigue properties are lower when compared to other materials. In particular, their ultimate and elastic properties rapidly decrease in a nonlinear fashion as the loading cycle increases[52,53]. Fatigue tests are usually achieved by stressing samples at a given value that has been considered to be the average or maximal stress which a given structure usually undergoes during functioning. In this sense, the FEA can be used to successfully estimate the stress to be applied to a given structure in order to simulate a desired fatigue condition.

CONCLUSION

Within the limitations of the present comparative FEA, the following conclusions were drawn:

(1) The comparable strain and stress levels recorded in both the roots and crowns of MOD 2, 3, and 4 suggested that post length exerted

no influence on the biomechanics of restored teeth.

(2) Compressive stress prevailed over tensile stress within the post structure, and that the latter could be considered negligible. Similarly, this phenomenon was not affected by the insertion length of posts inside the root.

REFERENCES

1) Yeh CJ. Fatigue root fracture: a spontaneous root fracture in non-endodontically treated teeth. Br Dent J 1997; 182: 261-266.
2) Ferrari M, Vichi A, Mannocci F, Mason PN. Retrospective study of the clinical performance of posts. Am J Dent 2000; 13: 9B-14B.
3) Guzy GE, Nicholls JI. *In vitro* comparison of intact endodontically treated teeth with and without endo-post reinforcement. J Prosthet Dent 1979; 42: 39-44.
4) Heydecke G, Butz F, Strub JR. Fracture strength and survival rate of endodontically treated maxillary incisors with approximal cavities restoration with different post and core systems: an *in vitro* study. J Dent 2001; 29: 427-433.
5) Troedson M, Derand T. Effect of margin design, cement polymerization, and angle of loading on stress in porcelain veneers. J Prosthet Dent 1999; 82: 518-524.
6) Huysmans MC, Van der Varst PG. Finite element analysis of quasi-static and fatigue of post and cores. J Dent 1993; 21: 57-64.
7) Akkayan B, Gulmez T. Resistance to fracture of endodontically treated teeth restored with different post systems. J Prosthet Dent 2002; 87: 431-437.
8) Lanza A, Aversa R, Rengo S, Apicella D, Apicella A. 3D FEA of cemented steel, glass and carbon posts in a maxillary incisor. Dent Mater 2005; 21: 709-715.
9) Sorrentino R, Monticelli F, Goracci C, Zarone F, Tay FR, Ferrari M. Effect of post and core restorations on the fracture resistance of endodontically treated maxillary premolars in different restorative systems. Am J Dent 2007; 20: 269-274.
10) Sorrentino R, Salameh Z, Zarone F, Tay FR, Ferrari M. Effect of post retained composite restorations of mesial-occlusal-distal cavities on the fracture resistance of endodontically treated teeth. J Adhes Dent 2007; 9: 49-56.
11) Sorrentino R, Aversa R, Ferro V, Auriemma T, Zarone F, Ferrari M, Apicella A. Three-dimensional finite element analysis of strain and stress distributions in endodontically treated maxillary central incisors restored with different post, core and crown materials. Dent Mater 2007; 23: 983-993.
12) Peters MCRB, Poort HW, Farah JW, Craig RG. Stress analysis of tooth restored with post and core. J Dent Res 1983; 62: 760-763.
13) Ortega VL, Pegoraro LF, Conti PCR, Do Valle AL, Bonfante G. Evaluation of fracture resistance of endodontically treated maxillary premolars, restored with Ceromer or heat-pressed ceramic inlays and fixed with dual-resin cements. J Oral Rehabil 2004; 31: 393-397.
14) Morgano SM. Restoration of pulpless teeth: application of traditional principles in present and future context. J Prosthet Dent 1996; 75: 375-380.
15) Innella R, Autieri G, Ceruti P, Gassino G. Relation between length of fiber post and its mechanical retention. An *in vitro* study. Minerva Stomatologica 2005; 54: 481-488.
16) Johnson JK, Sakumura JS. Dowel form and tensile force. J Prosthet Dent 1978; 40: 645-649.
17) Asmussen E, Peutzfeldt A, Sahafi A. Finite element analysis of stresses in endodontically treated, dowel-restored teeth. J Prosthet Dent 2005; 94: 321-329.
18) Goodacre CJ, Spolnik KJ. The prosthodontic management of endodontically treated teeth: a literature review. Part II: Maintaining the apical seal. J Prosthodont 1995; 4: 51-53.
19) Abramovitz L, Lev R, Fuss Z, Metzger Z. The unpredictability of seal after post space preparation: a fluid transport study. J Endod 2001; 27: 292-295.
20) Ausiello P, Apicella A, Davidson CL, Rengo S. 3D finite elements analysis of cusp movements in a human upper premolar, restored with adhesive resin-based composites. J Biomech 2001; 34: 1269-1277.
21) Dalstra M, Huiskes R, van Erning L. Development and validation of a three-dimensional finite element model of the pelvic bone. J Biomech Eng 1995; 117: 272-278.
22) Zarone F, Apicella A, Nicolais L, Aversa R, Sorrentino R. Mandibular flexure and stress build-up in mandibular full-arch fixed prostheses supported by osseointegrated implants. Clin Oral Impl Res 2003; 1: 319-328.
23) Yang HS, Lang LA, Molina A, Felton DA. The effects of dowel design and load direction on dowel-and-core restorations. J Prosthet Dent 2001; 85: 558-567.
24) Toparli M. Stress analysis in a post-restored tooth utilizing the finite element method. J Oral Rehabil 2003; 30: 470-476.
25) De Castro Albuquerque R, De Abreu Polleto LT, Fontana RHBTS, Cimini Jr CA. Stress analysis of an upper central incisor restored with different posts. J Oral Rehabil 2003; 30: 936-943.
26) Pierrisnard L, Bohin F, Renault P, Barquins M. Corono-radicular reconstruction of pulpless teeth: a mechanical study using finite element analysis. J Prosthet Dent 2002; 88: 442-448.
27) Ona M, Wakabayashi N. Influence of alveolar support on stress in periodontal structures. J Dent Res 2006; 85: 1087-1091.
28) Katranji A, Misch K, Wang HL. Cortical bone thickness in dentate and edentulous human cadavers. J Periodontol 2007; 78: 874-878.
29) Natali AN, Pavan PG, Scarpa C. Numerical analysis of tooth mobility: formulation of a non-linear constitutive law for the periodontal ligament. Dent Mater 2004; 20: 623-629.
30) Farah JV, Craig RG, Meroueh KA. Finite element analysis of three- and four-unit bridges. J Oral Rehabil 1989; 16: 603-611.
31) Matsushita Y, Kihara M, Koyano K, Murakami Y. Evaluation of Young's modulus of human mandible by ultra-micro indentation method. J Jap Soc

Biomater 2000; 18: 247-252.
32) O'Mahony AM, Williams JL, Katz JO, Spencer P. Anisotropic elastic properties of cancellous bone from an human edentoulus mandible. Clin Oral Implants Res 2000; 11: 415-421.
33) Joshi S, Mukherjee A, Kheur M, Mehta A. Mechanical performance of endodontically treated teeth. Finite Elements in Analysis and Design 2001; 37: 587-601.
34) Ho SP, Goodis H, Balooch M, Marshall SJ, Marshall G. Ultrastructure and nanomechanical properties of cementum enamel junction. J Biomed Mater Res A 2004; 68: 343-351.
35) Kinney JH, Marshall SJ, Marshall GW. The mechanical properties of human dentine: a critical review and re-evaluation of the dental literature. Crit Rev Oral Biol Med 2000; 14: 13-29.
36) Decraemer WF, Maes MA, Vanhuyse VJ, Vanpeperstraete P. A non-linear viscoelastic constitutive equation for soft biological tissues, based upon a structural model. J Biomech 1980; 13: 559-564.
37) Van Driel WD, van Leewen EJ, Von den Hoff JW, Maltha JC, Kuijpers-Jagtman AM. Time-dependent mechanical behavior of the periodontal ligament. Proc Inst Mech Eng 2000; 214: 407-504.
38) Colin SS, Wiskott HWA, Justiz J, Botsis J, Belser UC. *In vitro* time-dependent response of periodontal ligament to mechanical loading. J Appl Physiol 2005; 99: 2369-2378.
39) Berkovitz B. The structure of the periodontal ligament: an update. Eur J Orthod 1990; 12: 51-76.
40) Pini M, Wiskott HW, Scherrer SS, Botsis J, Belser UC. Mechanical characterization of bovine periodontal ligament. J Periodontal Res 2002; 37: 237-244.
41) Pini M, Zysset P, Botsis J, Contro R. Tensile and compressive behavior of the bovine periodontal ligament. J Biomech 2004; 37: 111-119.
42) Shibata T, Botsis J, Bergomi M, Mellal M, Komatsu K. Mechanical behavior of bovine periodontal ligament under tension-compression cyclic displacements. Eur J Oral Sci 2006; 114: 74-82.
43) Halpin JC, Kardos JL. The Halpine-Tsai equations: a review. Polym Eng and Sci 1976; 16: 344-352.
44) Ausiello P, Apicella A, Davidson CL. Effect of adhesive layer properties on stress distribution in composite restorations: a 3D finite element analysis. Dent Mater 2002; 18: 295-303.
45) Parfitt GJ. Measurement of the physiological mobility of individual teeth in an axial direction. J Dent Res 1960; 39: 608-618.
46) Muhlemann HR. Periodontometry, a method for measuring tooth mobility. Oral Surg Oral Med Oral Pathol 1951; 4: 1220-1233.
47) Tsai J, Sun CT. Dynamic compressive strengths of polymeric composites. Int J Solids Struct 2004; 41: 3211-3224.
48) Seefeld F, Wenz HJ, Ludwig K, Kern M. Resistance to fracture and structural characteristics of different fiber reinforced post systems. Dent Mater 2007; 23: 265-271.
49) Dietschi D, Romelli M, Goretti A. Evaluation of post and core in the laboratory: rationale for developing a fatigue test and preliminary results. Compend Cont Educ Dent Suppl 1996; 20: s65-s73.
50) Dietschi D, Romelli M, Goretti A. Adaptation of adhesive posts and core to dentin after fatigue testing. Int J Prosthodont 1997; 10: 498-507.
51) Hsu YB, Nicholls JL, Philips KM, Libman WJ. Effect of core bonding on fatigue failure of compromised teeth. Int J Prosthodont 2002; 15: 175-178.
52) Ferreira JM, Pires JTB, Costa JD, Errajhi OA, Richardson M. Fatigue damage and environment interaction of polyester aluminized glass fiber composites. Comp Struct 2007; 78: 397-401.
53) Sakin R, Ay I, Yaman R. An investigation of bending fatigue behavior for glass fiber-reinforced polyester composite materials. Materials and Design 2008; 29: 212-217.